

The time dimensional reduction method to determine the initial conditions for nonlinear and nonlocal hyperbolic equations

Trong D. Dang* Loc H. Nguyen† Huong T. T. Vu‡

Abstract

The objective of this paper is to compute initial conditions for quasi-linear hyperbolic equations. Our proposed approach involves approximating the solution of the hyperbolic equation by truncating its Fourier expansion in the time domain using the polynomial-exponential basis. This truncation enables the elimination of the time variable, resulting in a system of quasi-linear elliptic equations. Thus, we refer to our approach as the “time dimensional reduction method.” To solve this system globally without requesting a good initial guess, we employ the Carleman contraction principle. To demonstrate the effectiveness of our method, we provide several numerical examples. The time dimensional reduction method not only provides accurate solutions but also exhibits exceptional computational speed.

Key words: numerical methods; Carleman estimate; contraction principle; globally convergent numerical method, quasi-linear hyperbolic equations.

AMS subject classification: 35R30; 65M32.

1 Introduction

Let Ω be an open and bounded domain of \mathbb{R}^d . Assume the Ω has a smooth boundary. Let T be a positive number that represents the final time. Let \mathcal{F} be an operator acting on $C^2(\bar{\Omega} \times [0, T])$ defined as

$$\mathcal{F}(v)(\mathbf{x}, t) = F\left(\mathbf{x}, t, v, \nabla v, v_t, \int_0^t K(s)v(\mathbf{x}, s)ds\right) \quad (1.1)$$

for all $(\mathbf{x}, t) \in \bar{\Omega} \times [0, T]$ where the kernel $K : \mathbb{R} \rightarrow \mathbb{R}$ and the map $F : \bar{\Omega} \times [0, T] \times \mathbb{R} \times \mathbb{R}^d \times \mathbb{R} \times \mathbb{R} \rightarrow \mathbb{R}$ are given. Let $u = u(\mathbf{x}, t)$ be the solution to the following initial value problem

$$\begin{cases} u_{tt} = \Delta u + \mathcal{F}(u) & (\mathbf{x}, t) \in \Omega \times (0, T), \\ u(\mathbf{x}, t) = 0 & (\mathbf{x}, t) \in \partial\Omega \times (0, T), \\ u(\mathbf{x}, 0) = g(\mathbf{x}) & \mathbf{x} \in \Omega, \\ u_t(\mathbf{x}, 0) = 0 & \mathbf{x} \in \Omega. \end{cases} \quad (1.2)$$

Here, $g : \bar{\Omega} \rightarrow \mathbb{R}$ is a smooth function. The inverse problem we are interested in is formulated as follows.

*Faculty of Mathematics and Computer Science, University of Science, Vietnam National University, Ho Chi Minh City, Vietnam, ddtrong@hcmus.edu.vn.

†Department of Mathematics and Statistics, University of North Carolina at Charlotte, Charlotte, NC, 28223, USA, loc.nguyen@charlotte.edu, corresponding author.

‡Department of Information Technology, University of Finance-Marketing, Ho Chi Minh City, Vietnam, vtthuong@ufm.edu.vn.

Problem 1.1 (An inverse source problem for quasi-linear nonlocal hyperbolic equation). *Given the boundary data*

$$h(\mathbf{x}, t) = \partial_\nu u(\mathbf{x}, t) \quad \text{for all } (\mathbf{x}, t) \in \partial\Omega \times (0, T), \quad (1.3)$$

compute the function $g(\mathbf{x})$ for $\mathbf{x} \in \Omega$.

Determining the optimal conditions that ensure the existence and uniqueness of solutions for a general problem like (1.2) poses a significant challenge. Investigation of these properties for (1.2) is beyond the scope of this paper, and we treat them as given assumptions. For completeness, we offer a set of conditions for \mathbf{p} and F that ensure the well-posedness of (1.2). We assume that \mathbf{p} is smooth with compact support, and F does not depend on the first derivatives of u . Furthermore, it is assumed that $|\mathcal{F}u| \leq C_1|u| + C_2$ for all functions $u \in H^2(\Omega \times (0, T))$, where C_1 and C_2 are positive constants. In this scenario, the unique solvability for (1.2) can be achieved by applying [6, Theorem 10.14], a theorem originally proven by Lions in [44]. For further information on the well-posedness of (1.2) in linear cases, we recommend the esteemed texts [10, 37].

Problem 1.1 can be viewed as the nonlinear variant of a critical problem originating from biomedical imaging, known as thermo/photo-acoustic tomography. The experimental setup leading to this problem involves directing non-ionizing laser pulses or microwaves at the biological tissue under examination (such as a woman’s breast in mammography), as detailed in [35, 36, 51]. A portion of this energy is absorbed and converted into heat, leading to thermal expansion and the subsequent emission of ultrasonic waves. Measurements of the ultrasonic pressures on a surface surrounding the tissue can provide insight into the structure inside the tissue. The existing techniques for resolving thermo/photo-acoustic tomography are primarily designed for linear hyperbolic equations. These include explicit reconstruction formulas in free space [9, 11, 46, 49], the time reversal method [18, 15, 16, 54, 55], the quasi-reversibility method [8, 42], and iterative methods [17, 52, 53]. These publications examine thermo/photo-acoustic tomography for straightforward models of non-damping and isotropic media. More complex models incorporating a damping or attenuation term can be found in [4, 3, 12, 2, 7, 14, 33, 34, 45]. The nonlinear case has been addressed in the paper [48], where the authors used the Carleman estimate and the contraction principle to tackle non-linearity. Like [48], we again employ these two tools to solve Problem 1.1. The new ingredient in this paper compared to [48] is the time-dimensional reduction, which is the truncation of the Fourier expansion with respect to time. As a result, the solver in the present paper can handle a broader range of nonlinearity, and it significantly improves computational efficiency. Moreover, the time-reduction technique helps enhance the convergence rate with respect to noise. The rate of convergence in [48] is of Hölder type while reducing the time domain helps regularize the inverse problem, leading to a Lipschitz convergence.

Traditional methods to tackle nonlinear inverse problems rely on optimization. However, these methods are local in the sense that they provide reliable solutions when good initial estimates of the solutions are available. The issue of local convergence is not always guaranteed unless certain additional conditions are met. For a condition that ensures the local convergence of the optimization method using Landweber iteration, we draw the reader’s attention to [13]. The task of computing solutions to nonlinear problems without needing a reliable initial guess is a compelling, challenging, and important problem in the scientific community. A general framework to solve nonlinear inverse problems on a global scale is known as convexification. The central concept of the convexification method involves using appropriate Carleman weight functions to convexify the mismatch functional. This phenomenon of convexification is rigorously demonstrated through the well-known Carleman estimates. Since its first introduction in [26], various versions of the convexification method have

been developed [5, 21, 22, 23, 24, 27, 29, 28, 31, 41]. In particular, the convexification method has been successfully applied with experimental data for the inverse scattering problem in the frequency domain, given only back scattering data [19, 20, 28]. Despite its effectiveness, the convexification method does have a downside - it is time-consuming. Inspired by this, we make use of the techniques in [39, 40, 47] to propose a new method based on Fourier expansion, fixed-point iteration, the contraction principle, and a suitable Carleman estimate to solve nonlinear inverse problems on a global scale. By "global," we mean that our method does not need a close approximation of the true solution as the initial guess.

Our method involves the following main ingredients:

1. Time reduction. We propose to cut off the Fourier expansion of the solution to (1.2) using a polynomial-exponential basis in the time domain. This step is crucial in transforming a problem of dimension $d + 1$ into a d -dimensional problem, enhancing computational speed. Additionally, it enables us to solve Problem 1.1 even when the nonlinearity F depends on a "memory" term, such as the Volterra integral in (1.1).
2. The fixed point-like iteration. Once the time domain is reduced, we obtain a system of quasi-linear elliptic equations. Our strategy for solving this system is to rewrite it as the equation $\Phi(x) = x$, where Φ represents an operator including specific Carleman weight functions. We can employ Carleman estimates to show that Φ is a contraction mapping. Consequently, the computed fixed point of Φ directly provides the desired solution to the inverse problem.

The strengths of our new approach include the facts that

1. it does not require a good initial guess;
2. it is quite general in the sense that no special structure is imposed on the nonlinearity F ;
3. the rate of convergence is fast.

The paper is organized as follows. In Section 2, we present the time dimensional reduction method. In Section 3, we construct a map and show that this map is contractive. In Section 4, we show the fixed point of the contraction mapping above approximates of the true solution we want to compute. Section 5 is to present some numerical examples. Section 6 is for concluding remarks.

2 The time dimensional reduction model

Let $\{\Psi_n\}_{n \geq 1}$ be the polynomial-exponential basis, introduced in [25], see also [50] for the high-dimensional version. The basis $\{\Psi_n\}_{n \geq 1}$ is constructed as follows. For $n \geq 1$, define $\phi(t) = t^{n-1}e^{t-T/2}$, $t \in (0, T)$. It is obvious that $\{\phi_n\}_{n \geq 1}$ is complete in $L^2(0, T)$. By applying the Gram-Schmidt orthogonalization process to the set $\{\phi_n\}_{n \geq 1}$, we obtain the polynomial basis $\{\Psi_n\}_{n \geq 1}$. The orthogonal basis of $\{\Psi_n\}_{n \geq 1}$ in $L^2(0, T)$ possesses a distinctive property that $\Psi'_n(t)$ is not identically zero for all n . This property plays a significant role in the time-dimensional reduction method, which will be discussed in detail later.

In order to propose a numerical method for solving Problem 1.1, it is permissible to approximate the wave function $u(\mathbf{x}, t)$ by truncating its Fourier series as follows:

$$u(\mathbf{x}, t) = \sum_{n=1}^{\infty} u_n(\mathbf{x})\Psi_n(t) \simeq \sum_{n=1}^N u_n(\mathbf{x})\Psi_n(t) \quad (2.1)$$

where N is a cutoff number determined by the given data, see Section 5 for our data-driven method to find N . The Fourier coefficient u_n in (2.1) is given by

$$u_n(\mathbf{x}) = \int_0^T u(\mathbf{x}, t) \Psi_n(t) dt, \quad n \geq 1. \quad (2.2)$$

By substituting the approximation (2.1) into the governing hyperbolic equation in (1.2), we obtain the following equation

$$\sum_{n=1}^N u_n(\mathbf{x}) \Psi_n''(t) = \sum_{n=1}^N \Delta u_n(\mathbf{x}) \Psi_n(t) + \mathcal{F} \left(\sum_{n=1}^N u_n(\mathbf{x}) \Psi_n(t) \right) \quad (2.3)$$

for $(\mathbf{x}, t) \in \Omega \times (0, T)$. By multiplying both sides of (2.3) by $\Psi_m(t)$ for each $m \in \{1, \dots, N\}$ and integrating the resulting equation, we arrive at

$$\sum_{n=1}^N s_{mn} u_n(\mathbf{x}) = \Delta u_m(\mathbf{x}) + \mathbf{f}_m U, \quad m \in \{1, 2, \dots, N\} \quad (2.4)$$

for $\mathbf{x} \in \Omega$, where

$$\begin{aligned} U(\mathbf{x}) &= (u_1, u_2, \dots, u_N)^T, \\ \mathbf{f}_m U(\mathbf{x}) &= \mathcal{F} \left(\sum_{n=1}^N u_n(\mathbf{x}) \Psi_n(t) \right) \Psi_m(t) dt, \\ s_{mn} &= \int_0^T \Psi_n''(t) \Psi_m(t) dt. \end{aligned}$$

Defining $\mathbf{F}U = (\mathbf{f}_1 U, \dots, \mathbf{f}_N U)^T$ and $S = (s_{mn})_{m,n=1}^N$, we can rewrite the system (2.4) as the form

$$\Delta U(\mathbf{x}) - SU(\mathbf{x}) + \mathbf{F}U(\mathbf{x}) = 0 \quad \text{for all } \mathbf{x} \in \Omega. \quad (2.5)$$

We next derive the boundary conditions for the vector U . It follows from the Dirichlet boundary condition in (1.2) that for each $m \in \{1, \dots, N\}$ that for all $\mathbf{x} \in \partial\Omega$,

$$u_m(\mathbf{x}) = 0. \quad (2.6)$$

We can compute the Neumann condition $\partial_\nu U(\mathbf{x})$ from the given boundary data (1.3) as

$$\partial_\nu u_m(\mathbf{x}) = \int_0^T h(\mathbf{x}, t) \Psi_m(t) dt \quad (2.7)$$

for all $m \in \{1, \dots, N\}$, $\mathbf{x} \in \partial\Omega$.

In summary, denote by

$$\mathbf{h}(\mathbf{x}) = \left(\int_0^T h(\mathbf{x}, t) \Psi_m(t) dt \right)_{m=1}^N, \quad \mathbf{x} \in \partial\Omega \quad (2.8)$$

the indirect data that can be computed from the given data in (1.3). By (2.5), (2.6) and (2.7), we have derived a system of quasi-linear elliptic equations for the vector U

$$\begin{cases} \Delta U(\mathbf{x}) - SU(\mathbf{x}) + \mathbf{F}U(\mathbf{x}) = 0 & \mathbf{x} \in \Omega, \\ U(\mathbf{x}) = 0 & \mathbf{x} \in \partial\Omega, \\ \partial_\nu U(\mathbf{x}) = \mathbf{h}(\mathbf{x}) & \mathbf{x} \in \partial\Omega. \end{cases} \quad (2.9)$$

The inverse source problem under consideration is reduced to the problem solving (2.9). Having the computed solution $U^{\text{comp}} = (u_1^{\text{comp}}, \dots, u_N^{\text{comp}})$ to (2.9) in hand, due to (2.1), we can find the computed source function g^{comp} by

$$g^{\text{comp}}(\mathbf{x}) = u^{\text{comp}}(\mathbf{x}, 0) = \sum_{n=1}^N u_n(\mathbf{x})\Psi_n(0) \quad \text{for all } \mathbf{x} \in \Omega. \quad (2.10)$$

Remark 2.1. *The technique we employ, which entails removing the time variable t from equation (1.2) to obtain (2.9), is known as the “time-dimensional reduction method.” The quasi-linear system (2.9) is called the “time-reduction model” associated with (1.2). By eliminating the dimension associated with the time variable, we achieve a substantial reduction in computational costs. In fact, we solve problem (2.9) in d dimensions, while the initial problem (1.2), prior to time reduction, exists in $d + 1$ dimensions, consisting of d spatial dimensions along with the time variable.*

Remark 2.2 (The significance of the polynomial-exponential basis). *The significance of the polynomial-exponential basis employed in the time reduction method is discussed here. It may raise the question of why we specifically chose the basis $\{\Psi_n\}_{n \geq 1}$, out of countless others, for the Fourier expansion in equation (2.1). The reason behind this selection is that commonly used bases, such as Legendre polynomials or trigonometric functions, may not be suitable in this context. The issue arises from the fact that the initial function of these bases is a constant, resulting in its derivative being identically zero. As a consequence, the corresponding Fourier coefficient $u_1(x)$ in the sums $\sum_{n=1}^N u_n(\mathbf{x})\Psi_n''(t)$ in equation (2.3) is neglected, leading to diminished accuracy. In contrast, the polynomial-exponential basis employed in this paper is well-suited for equation (2.3) since it satisfies the necessary condition that Ψ_n' , for $n \geq 1$, is not identically zero.*

The effectiveness of the polynomial-exponential basis has been demonstrated in various studies, including [42, 50]. In [42], we utilized the polynomial-exponential and traditional trigonometric bases to expand wave fields and address problems in photo-acoustic and thermo-acoustic tomography. The results clearly indicated superior performance by the polynomial-exponential basis. Additionally, in [50], we applied Fourier expansion to compute derivatives of data corrupted by noise. The outcomes demonstrated that the polynomial-exponential basis exhibited higher accuracy compared to the trigonometric basis when performing term-by-term differentiation of the Fourier expansion to solve ill-posed problems. Consequently, when term-by-term differentiation of the Fourier expansion is required, the polynomial-exponential basis should be utilized due to its favorable properties and demonstrated advantages.

Remark 2.3. *Recall that upon solving the time-reduction model (2.9), the solution to Problem 1.1 can be computed using (2.10). As the time-reduction model (2.9) relies on the cutoff number N , studying the convergence of our method as N tends to infinity poses significant challenges. However, addressing this question is beyond the scope of this paper, as our primary focus lies in the computational aspects.*

There are several methods to solve the time-reduction model (2.9). We list some options below

1. The least squares optimization method: This method is widely employed in the scientific community, where a cost functional is established, and the computed solution is set as the global minimizer of the functional. An example of such a functional is

$$V \mapsto J(v) := \int_{\Omega} |\Delta V(\mathbf{x}) - SV(\mathbf{x}) + \mathbf{F}V(\mathbf{x})|^2 d\mathbf{x} + \text{a regularization term}$$

subject to the boundary conditions $V = \mathbf{f}$ and $\partial_\nu V = \mathbf{h}$ on $\partial\Omega$. Finding the global minimizer of J can be challenging due to the potential existence of multiple local minimizers. Reliable solutions using the optimization method often require a good initial guess close to the true solution.

2. The convexification method: Initially introduced in [26], this method allows for solving inverse problems without necessitating a good initial guess. Various versions of the convexification method have been developed and explored in subsequent papers [5, 19, 20, 21, 25, 30, 32, 38, 41].
3. The Carleman contraction method [47] along with the recently developed Carleman-Newton method [1, 43], can provide reliable solutions to (2.9) without requiring an initial guess. These methods offer faster convergence rates compared to the convexification method. In this paper, we generalize the Carleman contraction method in [47] to solve (2.9). This will be presented in Section 3.

The key aspect shared by the convexification, Carleman contraction, and Carleman-Newton methods is the inclusion of Carleman weight functions within the procedure. The efficacy of these approaches is demonstrated using Carleman estimates.

3 The Carleman contraction mapping

Let $p > [d/2] + 2$ be an integer. Define the functional space

$$H = \{\varphi \in H^p(\Omega)^N : \varphi|_{\partial\Omega} = 0\}. \quad (3.1)$$

It is obvious that H is a closed subspace of the Hilbert space $H^p(\Omega)^N$. Let \mathbf{x}_0 be a point in $\mathbb{R}^d \setminus \bar{\Omega}$ such that $r(\mathbf{x}) = |\mathbf{x} - \mathbf{x}_0| > 1$ for all $\mathbf{x} \in \Omega$. For each $\epsilon > 0$, $\lambda > 0$ and $\beta > 0$, introduce the map

$$\Phi_{\lambda,\beta,\epsilon} : H \rightarrow H, \quad W \mapsto \Phi_{\lambda,\beta,\epsilon}(W) = \underset{V \in H}{\operatorname{argmin}} J_{\lambda,\beta,\epsilon}^W(V) \quad (3.2)$$

where

$$J_{\lambda,\beta,\epsilon}^W(V) = \int_{\Omega} e^{2\lambda r^{-\beta}} |\Delta V - SV + \mathbf{F}(W)|^2 d\mathbf{x} + \lambda^2 \int_{\partial\Omega} e^{2\lambda r^{-\beta}} |\partial_\nu V - \mathbf{h}|^2 d\sigma(\mathbf{x}) + \epsilon \|V\|_H^2 \quad (3.3)$$

for all $V \in H$. The existence and uniqueness of $J_{\lambda,\beta,\epsilon}$ is obvious. For each fix $W \in H$, $J_{\lambda,\beta,\epsilon}^W(V)$ is strictly convex in Hilbert space H . In other words, the map $\Phi_{\lambda,\beta,\epsilon}$ is well-defined, see also [47, Remark 3.1]. As mentioned in the last paragraph of Section 2, the presence of the Carleman weight function $e^{2\lambda r^{-\beta}}$ in the integral in the right-hand side of (3.3) is the main point of our globally convergent method to compute a numerical solution to (2.9).

Assume that F is Lipschitz; i.e., there is a constant M_F such that

$$|F(\mathbf{x}, t, s_1, \mathbf{p}_1, r_1, l_1) - F(\mathbf{x}, t, s_2, \mathbf{p}_2, r_2, l_2)| \leq M_F(|s_1 - s_2| + |\mathbf{p}_1 - \mathbf{p}_2| + |r_1 - r_2| + |l_1 - l_2|) \quad (3.4)$$

for all $\mathbf{x} \in \bar{\Omega}$, $s_i \in \mathbb{R}$, $\mathbf{p}_i \in \mathbb{R}^d$, $r_i \in \mathbb{R}$, $l_i \in \mathbb{R}$, $i \in \{1, 2\}$. Then, we can find a constant \mathbf{M} depending on M_F , K , $\{\Psi_n\}_{n=1}^N$, N and T such that

$$|\mathbf{F}(V_1) - \mathbf{F}(V_2)|^2 \leq \mathbf{M}(|V_1 - V_2|^2 + |\nabla V_1 - \nabla V_2|^2) \quad (3.5)$$

for all vector-valued functions V_1 and V_2 and for all $(\mathbf{x}, t) \in \overline{\Omega} \times [0, T]$. For $\lambda > 0$, $\beta > 0$, and $\varepsilon > 0$, define the norm $\|\cdot\|_{\lambda, \beta, \varepsilon}$

$$\|U\|_{\lambda, \beta, \varepsilon} = \left(\int_{\Omega} e^{2\lambda r^{-\beta}} (\lambda^2 |U|^2 + |\nabla U|^2) d\mathbf{x} + \lambda \int_{\partial\Omega} e^{2\lambda r^{-\beta}} |\nabla U|^2 d\sigma(\mathbf{x}) + \frac{\varepsilon}{\lambda} \|U\|_H^2 \right)^{1/2} \quad (3.6)$$

for all $U \in H$. We have the theorems.

Theorem 3.1. *Assume (3.4) and hence (3.5) hold true. Then, there is a constant β_0 depending only on \mathbf{M} , d , Ω , and \mathbf{x}_0 such that for all $\beta \geq \beta_0$, we have*

$$\|\Phi_{\lambda, \beta, \varepsilon}(U) - \Phi_{\lambda, \beta, \varepsilon}(V)\|_{\lambda, \beta, \varepsilon} \leq \sqrt{\frac{C}{\lambda}} \|U - V\|_{\lambda, \beta, \varepsilon} \quad (3.7)$$

for all $\lambda > \lambda_0$ where $\lambda_0 = \lambda_0(\mathbf{M}, d, \Omega, d, \mathbf{x}_0, \beta)$ and $C = C(\mathbf{M}, d, \Omega, d, \mathbf{x}_0, \beta)$ depending only on the listed parameters. Consequently, choosing $\lambda > \lambda_0$ sufficiently large, the map $\Phi_{\lambda, \beta, \varepsilon} : H \rightarrow H$ is a contraction mapping with respect to the norm $\|\cdot\|_{\lambda, \beta, \varepsilon}$.

The following result is a point-wise Carleman estimate, which plays a pivotal role in the proof of Theorem 3.1 and the convergence of our method with respect to the noise in the next section.

Lemma 3.1 (See Theorem 3.1 in [38]). *Let $\lambda > 0$ and $v \in C^2(\overline{\Omega})$. Then, there exists a positive constant β_0 depending only on \mathbf{x}_0 , d and Ω such that for all $\beta \geq \beta_0$ and $\lambda \geq \lambda_0 = 2R^\beta$, where $R = \max_{\mathbf{x} \in \overline{\Omega}} \{|\mathbf{x} - \mathbf{x}_0|\}$, we have*

$$r^{\beta+2} e^{2\lambda r^{-\beta}} |\Delta v|^2 \geq C \left[\operatorname{div}(V) + \lambda^3 \beta^4 e^{2\lambda r^{-\beta}} r^{-2\beta-2} |v|^2 + \lambda \beta e^{2\lambda r^{-\beta}} |\nabla v|^2 \right]. \quad (3.8)$$

Here, V is a vector-valued function satisfying

$$|V| \leq C e^{2\lambda r^{-\beta}} (\lambda^3 \beta^3 r^{-2\beta-2} |v|^2 + \lambda \beta |\nabla v|^2) \quad (3.9)$$

and C is a constant depending only on \mathbf{x}_0 , Ω , and d .

We refer the reader to [38, Theorem 3.1] for the proof of this Carleman estimate. A direct consequence of (3.8) is as follows.

Corollary 3.1. *Let $v \in C^2(\overline{\Omega})$ with $v|_{\partial\Omega} = 0$. We have*

$$\int_{\Omega} e^{2\lambda r^{-\beta}} |\Delta v|^2 d\mathbf{x} \geq -C \lambda \int_{\partial\Omega} e^{2\lambda r^{-\beta}} |\nabla v|^2 d\sigma(\mathbf{x}) + C \int_{\Omega} e^{2\lambda r^{-\beta}} [\lambda^3 |v|^2 + \lambda |\nabla v|^2] d\mathbf{x} \quad (3.10)$$

for λ, β and C as in Lemma 3.1.

Proof. Integrating (3.8) and using integrating by parts, we have

$$\int_{\Omega} r^{\beta+2} e^{2\lambda r^{-\beta}} |\Delta v|^2 \geq C \int_{\partial\Omega} V \cdot \nu d\mathbf{x} + C \int_{\Omega} [\lambda^3 \beta^4 e^{2\lambda r^{-\beta}} r^{-2\beta-2} |v|^2 + \lambda \beta e^{2\lambda r^{-\beta}} |\nabla v|^2].$$

By (3.9), we have

$$\begin{aligned} \int_{\Omega} r^{\beta+2} e^{2\lambda r^{-\beta}} |\Delta v|^2 &\geq -C \int_{\partial\Omega} e^{2\lambda r^{-\beta}} (\lambda^3 \beta^3 r^{-2\beta-2} |v|^2 + \lambda \beta |\nabla v|^2) d\sigma(\mathbf{x}) \\ &\quad + C \int_{\Omega} [\lambda^3 \beta^4 e^{2\lambda r^{-\beta}} r^{-2\beta-2} |v|^2 + \lambda \beta e^{2\lambda r^{-\beta}} |\nabla v|^2]. \end{aligned}$$

Since $v|_{\partial\Omega} = 0$, we have

$$\begin{aligned} \int_{\Omega} r^{\beta+2} e^{2\lambda r^{-\beta}} |\Delta v|^2 d\mathbf{x} &\geq -C \int_{\partial\Omega} e^{2\lambda r^{-\beta}} \lambda \beta |\nabla v|^2 d\sigma(\mathbf{x}) \\ &\quad + C \int_{\Omega} [\lambda^3 \beta^4 e^{2\lambda r^{-\beta}} r^{-2\beta-2} |v|^2 + \lambda \beta e^{2\lambda r^{-\beta}} |\nabla v|^2], \end{aligned}$$

which directly implies (3.10). It should be noted that in the above argument, the constant C is allowed to depend on β , Ω , and \mathbf{x}_0 . \square

Proof of Theorem 3.1. Define $U_1 = \Phi_{\lambda, \beta, \epsilon}(U)$. By the definition of $\Phi_{\lambda, \beta, \epsilon}$ in (3.2), we have U_1 is the minimizer of $J_{\lambda, \beta, \epsilon}^U$ in H where $J_{\lambda, \beta, \epsilon}^U$ is defined in (3.3) with U replacing W . By the variational principle, for all $\varphi \in H$, we have

$$\begin{aligned} \langle e^{2\lambda r^{-\beta}} (\Delta U_1 - S U_1 + \mathbf{F}(U)), \Delta \varphi - S \varphi \rangle_{L^2(\Omega)^N} \\ + \lambda^2 \langle e^{2\lambda r^{-\beta}} (\partial_{\nu} U_1 - \mathbf{h}), \partial_{\nu} \varphi \rangle_{L^2(\partial\Omega)^N} + \epsilon \langle U_1, \varphi \rangle_H = 0. \end{aligned} \quad (3.11)$$

Similarly, set $V_1 = \Phi_{\lambda, \beta, \epsilon}(V)$. We have

$$\begin{aligned} \langle e^{2\lambda r^{-\beta}} (\Delta V_1 - S V_1 + \mathbf{F}(V)), \Delta \varphi - S \varphi \rangle_{L^2(\Omega)^N} \\ + \lambda^2 \langle e^{2\lambda r^{-\beta}} (\partial_{\nu} V_1 - \mathbf{h}), \partial_{\nu} \varphi \rangle_{L^2(\partial\Omega)^N} + \epsilon \langle V_1, \varphi \rangle_H = 0 \end{aligned} \quad (3.12)$$

for all $\varphi \in H$. Subtracting (3.12) from (3.11) gives

$$\begin{aligned} \langle e^{2\lambda r^{-\beta}} (\Delta(U_1 - V_1) - S(U_1 - V_1) + \mathbf{F}(U) - \mathbf{F}(V)), \Delta \varphi - S \varphi \rangle_{L^2(\Omega)^N} \\ + \lambda^2 \langle e^{2\lambda r^{-\beta}} \partial_{\nu}(U_1 - V_1), \partial_{\nu} \varphi \rangle_{L^2(\partial\Omega)^N} + \epsilon \langle U_1 - V_1, \varphi \rangle_H = 0 \end{aligned} \quad (3.13)$$

for all $\varphi \in H$. In particular, using $\varphi = U_1 - V_1$ in (3.13) gives

$$\begin{aligned} \int_{\Omega} e^{2\lambda r^{-\beta}} |\Delta \varphi - S \varphi|^2 d\mathbf{x} + \lambda^2 \int_{\partial\Omega} e^{2\lambda r^{-\beta}} |\partial_{\nu} \varphi|^2 d\sigma(\mathbf{x}) + \epsilon \|\varphi\|_H^2 \\ = \int_{\Omega} e^{2\lambda r^{-\beta}} (\Delta \varphi - S \varphi) (\mathbf{F}(U) - \mathbf{F}(V)) d\mathbf{x} \\ \leq \frac{1}{2} \int_{\Omega} e^{2\lambda r^{-\beta}} |\Delta \varphi - S \varphi|^2 d\mathbf{x} + \frac{1}{2} \int_{\Omega} e^{2\lambda r^{-\beta}} |\mathbf{F}(U) - \mathbf{F}(V)|^2 d\mathbf{x}. \end{aligned}$$

Hence,

$$\int_{\Omega} e^{2\lambda r^{-\beta}} |\Delta \varphi - S \varphi|^2 d\mathbf{x} + \lambda^2 \int_{\partial\Omega} e^{2\lambda r^{-\beta}} |\partial_{\nu} \varphi|^2 d\sigma(\mathbf{x}) + \epsilon \|\varphi\|_H^2 \leq C \int_{\Omega} e^{2\lambda r^{-\beta}} |\mathbf{F}(U) - \mathbf{F}(V)|^2 d\mathbf{x}. \quad (3.14)$$

It follows from (3.14) and the inequality $(a - b)^2 \leq \frac{1}{2}a^2 - b^2$ that

$$\begin{aligned} \int_{\Omega} e^{2\lambda r^{-\beta}} |\Delta \varphi|^2 d\mathbf{x} + \lambda^2 \int_{\partial\Omega} e^{2\lambda r^{-\beta}} |\partial_{\nu} \varphi|^2 d\sigma(\mathbf{x}) + \epsilon \|\varphi\|_H^2 \\ \leq C \left(\int_{\Omega} e^{2\lambda r^{-\beta}} |S \varphi|^2 d\mathbf{x} + \int_{\Omega} e^{2\lambda r^{-\beta}} |\mathbf{F}(U) - \mathbf{F}(V)|^2 d\mathbf{x} \right). \end{aligned} \quad (3.15)$$

Combining Carleman estimate (3.10) for φ and (3.15), we have

$$\begin{aligned} -C\lambda \int_{\Omega} e^{2\lambda r^{-\beta}} |\nabla\varphi|^2 d\sigma(\mathbf{x}) + C \int_{\Omega} e^{2\lambda r^{-\beta}} [\lambda^3 |\varphi|^2 + \lambda |\nabla\varphi|^2] d\mathbf{x} + \lambda^2 \int_{\partial\Omega} e^{2\lambda r^{-\beta}} |\partial\varphi|^2 d\sigma(\mathbf{x}) \\ + \epsilon \|\varphi\|_H^2 \leq C \left(\int_{\Omega} e^{2\lambda r^{-\beta}} |S\varphi|^2 d\mathbf{x} + \int_{\Omega} e^{2\lambda r^{-\beta}} |\mathbf{F}(U) - \mathbf{F}(V)|^2 d\mathbf{x} \right). \end{aligned} \quad (3.16)$$

Since $\varphi|_{\partial\Omega} = 0$, $|\nabla\varphi| = |\partial_\nu\varphi|$ on $\partial\Omega$. Since λ is large, the third integral on the left-hand side of equation (3.16) prevails over the first one. Moreover, the second integral on the left-hand side of equation (3.16) dominates the first integral on the right-hand side. Thus, we can deduce the following estimate

$$\begin{aligned} \int_{\Omega} e^{2\lambda r^{-\beta}} [\lambda^3 |\varphi|^2 + \lambda |\nabla\varphi|^2] d\mathbf{x} + \lambda^2 \int_{\partial\Omega} e^{2\lambda r^{-\beta}} |\partial\varphi|^2 d\sigma(\mathbf{x}) + \epsilon \|\varphi\|_H^2 \\ \leq C \int_{\Omega} e^{2\lambda r^{-\beta}} |\mathbf{F}(U) - \mathbf{F}(V)|^2 d\mathbf{x}. \end{aligned} \quad (3.17)$$

Recalling (3.5), we have

$$\begin{aligned} \lambda \left(\int_{\Omega} e^{2\lambda r^{-\beta}} [\lambda^2 |\varphi|^2 + |\nabla\varphi|^2] d\mathbf{x} + \lambda \int_{\partial\Omega} e^{2\lambda r^{-\beta}} |\partial\varphi|^2 d\sigma(\mathbf{x}) + \frac{\epsilon}{\lambda} \|\varphi\|_H^2 \right) \\ \leq C \int_{\Omega} e^{2\lambda r^{-\beta}} |U - V|^2 + |\nabla(U - V)|^2 d\mathbf{x} \\ \leq C \left(\int_{\Omega} e^{2\lambda r^{-\beta}} (\lambda^2 |U - V|^2 + |\nabla(U - V)|^2) d\mathbf{x} + \lambda \int_{\partial\Omega} e^{2\lambda r^{-\beta}} |\partial(U - V)|^2 d\sigma(\mathbf{x}) \right. \\ \left. + \frac{\epsilon}{\lambda} \|U - V\|_H^2 \right). \end{aligned}$$

The desired estimate (3.7) follows. \square

Remark 3.1. *The proof of Theorem 3.1 is similar to that of Theorem 3.1 in [47]. However, the key distinction lies in the inclusion of the boundary integral within the norm $\|\cdot\|_{\lambda,\beta,\epsilon}$, resulting the convergence with respect to a stronger norm. This modification allows for the investigation of noise analysis without the need to impose a technical condition that the noise is the restriction of a smooth function, see [47, Section 4].*

Define the sequence

$$\begin{cases} U_0 \in H \text{ be chosen arbitrarily,} \\ U_{n+1} = \Phi_{\lambda,\beta,\epsilon}(U_n) \end{cases} \quad n \geq 0 \quad (3.18)$$

A direct consequence of Theorem 3.1 is that the sequence $\{U_n\}_{n \geq 1}$ converges to a vector-valued function \bar{U} in H with respect to the norm $\|\cdot\|_{\lambda,\beta,\epsilon}$. In the next section, we will show that \bar{U} is a good approximation of the solution to (2.9).

4 The convergence of the Carleman contraction principle

We assume that the observed data $h = \partial_\nu u(\mathbf{x}, t)$, $(\mathbf{x}, t) \in \partial\Omega \times (0, T)$ contains noise. As a result, the indirect data for (2.9), the vector \mathbf{h} defined in (2.8) is not accurate. Denote by \mathbf{h}^* the exact version of the vector \mathbf{h} . Assume that problem (2.9) with \mathbf{h} being replaced with \mathbf{h}^* has a unique solution, denoted by U^* .

We have the theorem.

Theorem 4.1. *Assume that (3.4) and hence (3.5) hold true. Fix $\beta > \beta_0$ and $\lambda \geq \lambda_0$ sufficiently large where β_0 and λ_0 are as in Theorem 3.1 such that $\Phi_{\lambda,\beta,\epsilon}$ is a contraction mapping for all $\epsilon > 0$. Let \bar{U} be the fixed point of $\Phi_{\lambda,\beta,\epsilon}$. We have*

$$\begin{aligned} \int_{\Omega} e^{2\lambda r^{-\beta}} [\lambda^3 |\bar{U} - U^*|^2 + \lambda |\nabla(\bar{U} - U^*)|^2] d\mathbf{x} + \lambda^2 \int_{\partial\Omega} e^{2\lambda r^{-\beta}} |\nabla(\bar{U} - U^*)|^2 d\sigma(\mathbf{x}) \\ + \epsilon \|\bar{U} - U^*\|_H^2 \leq C \left[\lambda^2 \int_{\partial\Omega} e^{2\lambda r^{-\beta}} |\mathbf{h} - \mathbf{h}^*|^2 d\sigma(\mathbf{x}) + \epsilon \|U^*\|_H^2 \right]. \end{aligned} \quad (4.1)$$

where $C = C(\mathbf{M}, \beta, \mathbf{x}_0, d, \Omega)$ is a constant.

Proof of Theorem 4.1. It is well-known that the fixed point \bar{U} of $\Phi_{\lambda,\beta,\epsilon}$ is the limit of the sequence $\{U_n\}_{n \geq 0}$, defined in (3.18), with respect to the norm $\|\cdot\|_{\lambda,\beta,\epsilon}$. Fix $n \geq 1$. Since $U_{n+1} = \Phi_{\lambda,\beta,\epsilon}(U_n)$ is the minimizer of $J_{\lambda,\beta,\epsilon}^{U_n}$ in H , by the variational principle, for all $\varphi \in H$, we have

$$\begin{aligned} \langle e^{2\lambda r^{-\beta}} (\Delta U_{n+1} - S U_{n+1} + \mathbf{F}(U_n)), \Delta \varphi - S \varphi \rangle_{L^2(\Omega)^N} \\ + \lambda^2 \langle e^{2\lambda r^{-\beta}} (\partial_\nu U_{n+1} - \mathbf{h}), \partial_\nu \varphi \rangle_{L^2(\partial\Omega)^N} + \epsilon \langle U_{n+1}, \varphi \rangle_H = 0 \end{aligned} \quad (4.2)$$

On the other hand, since U^* is the solution to (2.9) with \mathbf{h}^* replacing \mathbf{h} , for all $\varphi \in H^p(\Omega)^N$, we have

$$\begin{aligned} \langle e^{2\lambda r^{-\beta}} (\Delta U^* - S U^* + \mathbf{F}(U^*)), \Delta \varphi - S \varphi \rangle_{L^2(\Omega)^N} \\ + \lambda^2 \langle e^{2\lambda r^{-\beta}} (\partial_\nu U^* - \mathbf{h}^*), \partial_\nu \varphi \rangle_{L^2(\partial\Omega)^N} + \epsilon \langle U^*, \varphi \rangle_H = \epsilon \langle U^*, \varphi \rangle_H \end{aligned} \quad (4.3)$$

for all $\varphi \in H$. Subtracting (4.2) from (4.3) and using

$$\varphi_{n+1} = U_{n+1} - U^* \in H \quad (4.4)$$

as the test function φ in (4.3), we have

$$\begin{aligned} \langle e^{2\lambda r^{-\beta}} (\Delta \varphi_{n+1} - S \varphi_{n+1} + \mathbf{F}(U_n) - \mathbf{F}(U^*)), \Delta \varphi_{n+1} - S \varphi_{n+1} \rangle_{L^2(\Omega)^N} \\ + \lambda^2 \langle e^{2\lambda r^{-\beta}} \partial_\nu \varphi_{n+1}, \partial_\nu \varphi_{n+1} \rangle_{L^2(\partial\Omega)^N} + \epsilon \langle \varphi_{n+1}, \varphi_{n+1} \rangle_H \\ = \lambda^2 \langle e^{2\lambda r^{-\beta}} \partial_\nu \varphi_{n+1}, \partial_\nu (\mathbf{h} - \mathbf{h}^*) \rangle_{L^2(\partial\Omega)^N} - \epsilon \langle U^*, \varphi_{n+1} \rangle_H. \end{aligned} \quad (4.5)$$

We can rewrite (4.5) as

$$\begin{aligned} \int_{\Omega} e^{2\lambda r^{-\beta}} |\Delta \varphi_{n+1} - S \varphi_{n+1}|^2 d\mathbf{x} + \lambda^2 \int_{\partial\Omega} e^{2\lambda r^{-\beta}} |\partial_\nu \varphi_{n+1}|^2 d\sigma(\mathbf{x}) + \epsilon \|\varphi_{n+1}\|_H^2 \\ = - \int_{\Omega} e^{2\lambda r^{-\beta}} (\mathbf{F}(U_n) - \mathbf{F}(U^*)) (\Delta \varphi_{n+1} - S \varphi_{n+1})^2 d\mathbf{x} \\ + \lambda^2 \int_{\partial\Omega} e^{2\lambda r^{-\beta}} \partial_\nu \varphi_{n+1} \cdot (\mathbf{h} - \mathbf{h}^*) d\sigma(\mathbf{x}) - \epsilon \langle U^*, \varphi_{n+1} \rangle_H. \end{aligned} \quad (4.6)$$

Using the inequality $|ab| \leq \frac{1}{2}(a^2 + b^2)$, we deduce from (4.6) that

$$\begin{aligned} \int_{\Omega} e^{2\lambda r^{-\beta}} |\Delta \varphi_{n+1} - S \varphi_{n+1}|^2 d\mathbf{x} + \lambda^2 \int_{\partial\Omega} e^{2\lambda r^{-\beta}} |\partial_\nu \varphi_{n+1}|^2 d\sigma(\mathbf{x}) + \epsilon \|\varphi_{n+1}\|_H^2 \\ \leq \int_{\Omega} e^{2\lambda r^{-\beta}} |\mathbf{F}(U_n) - \mathbf{F}(U^*)|^2 d\mathbf{x} + \lambda^2 \int_{\partial\Omega} e^{2\lambda r^{-\beta}} |\mathbf{h} - \mathbf{h}^*|^2 d\sigma(\mathbf{x}) + \epsilon \|U^*\|_H^2. \end{aligned} \quad (4.7)$$

Since $\varphi_{n+1}|_{\partial\Omega} = 0$, $|\partial_\nu \varphi_{n+1}| = |\nabla \varphi_{n+1}|$ on $\partial\Omega$. Also, due to the inequality $(a - b)^2 \geq \frac{1}{2}a^2 - b^2$, we obtain from (4.7) that

$$\begin{aligned} & \frac{1}{2} \int_{\Omega} e^{2\lambda r^{-\beta}} |\Delta \varphi_{n+1}|^2 d\mathbf{x} - \int_{\Omega} e^{2\lambda r^{-\beta}} |S\varphi_{n+1}|^2 d\mathbf{x} + \lambda^2 \int_{\partial\Omega} e^{2\lambda r^{-\beta}} |\nabla \varphi_{n+1}|^2 d\sigma(\mathbf{x}) + \epsilon \|\varphi_{n+1}\|_H^2 \\ & \leq \int_{\Omega} e^{2\lambda r^{-\beta}} |\mathbf{F}(U_n) - \mathbf{F}(U^*)|^2 d\mathbf{x} + \lambda^2 \int_{\partial\Omega} e^{2\lambda r^{-\beta}} |\mathbf{h} - \mathbf{h}^*|^2 d\sigma(\mathbf{x}) + \epsilon \|U^*\|_H^2. \end{aligned} \quad (4.8)$$

We now apply the Carleman estimate in (3.10) to estimate the left-hand side of (4.8). Combining (3.10) for the vector-valued function φ_{n+1} and (4.8), we obtain

$$\begin{aligned} & -C\lambda \int_{\partial\Omega} e^{2\lambda r^{-\beta}} |\nabla \varphi_{n+1}|^2 d\sigma(\mathbf{x}) + C \int_{\Omega} e^{2\lambda r^{-\beta}} [\lambda^3 |\varphi_{n+1}|^2 + \lambda |\nabla \varphi_{n+1}|^2] d\mathbf{x} - \int_{\Omega} e^{2\lambda r^{-\beta}} |S\varphi_{n+1}|^2 d\mathbf{x} \\ & + \lambda^2 \int_{\partial\Omega} e^{2\lambda r^{-\beta}} |\nabla \varphi_{n+1}|^2 d\sigma(\mathbf{x}) + \epsilon \|\varphi_{n+1}\|_H^2 \leq \int_{\Omega} e^{2\lambda r^{-\beta}} |\mathbf{F}(U_n) - \mathbf{F}(U^*)|^2 d\mathbf{x} \\ & + \lambda^2 \int_{\partial\Omega} e^{2\lambda r^{-\beta}} |\mathbf{h} - \mathbf{h}^*|^2 d\sigma(\mathbf{x}) + \epsilon \|U^*\|_H^2. \end{aligned} \quad (4.9)$$

Letting λ large, we can simplify (4.9) as

$$\begin{aligned} & \int_{\Omega} e^{2\lambda r^{-\beta}} [\lambda^3 |\varphi_{n+1}|^2 + \lambda |\nabla \varphi_{n+1}|^2] d\mathbf{x} + \lambda^2 \int_{\partial\Omega} e^{2\lambda r^{-\beta}} |\nabla \varphi_{n+1}|^2 d\sigma(\mathbf{x}) + \epsilon \|\varphi_{n+1}\|_H^2 \\ & \leq C \left[\int_{\Omega} e^{2\lambda r^{-\beta}} |\mathbf{F}(U_n) - \mathbf{F}(U^*)|^2 d\mathbf{x} + \lambda^2 \int_{\partial\Omega} e^{2\lambda r^{-\beta}} |\mathbf{h} - \mathbf{h}^*|^2 d\sigma(\mathbf{x}) + \epsilon \|U^*\|_H^2 \right]. \end{aligned} \quad (4.10)$$

We now employ the Lipschitz continuity of \mathbf{F} . It follows from (3.5) and (4.10) that

$$\begin{aligned} & \int_{\Omega} e^{2\lambda r^{-\beta}} [\lambda^3 |\varphi_{n+1}|^2 + \lambda |\nabla \varphi_{n+1}|^2] d\mathbf{x} + \lambda^2 \int_{\partial\Omega} e^{2\lambda r^{-\beta}} |\nabla \varphi_{n+1}|^2 d\sigma(\mathbf{x}) + \epsilon \|\varphi_{n+1}\|_H^2 \\ & \leq C \left[\mathbf{M} \int_{\Omega} e^{2\lambda r^{-\beta}} [|U_n - U^*|^2 + |\nabla(U_n - U^*)|^2] d\mathbf{x} \right. \\ & \quad \left. + \lambda^2 \int_{\partial\Omega} e^{2\lambda r^{-\beta}} |\mathbf{h} - \mathbf{h}^*|^2 d\sigma(\mathbf{x}) + \epsilon \|U^*\|_H^2 \right]. \end{aligned} \quad (4.11)$$

Recall from (4.4) that $\varphi_{n+1} = U_{n+1} - U^*$ and that $U_n \rightarrow \bar{U}$ in H with respect to the norm $\|\cdot\|_{\lambda, \beta, \epsilon}$. When the parameters λ , β , and ϵ are fixed, we can conclude that $U_n \rightarrow \bar{U}$ with respects to all of the norms $L^2(\Omega)$, $H^1(\Omega)$, and $H^p(\Omega)$. Letting n in (4.11) to ∞ , we have

$$\begin{aligned} & \int_{\Omega} e^{2\lambda r^{-\beta}} [\lambda^3 |\bar{U} - U^*|^2 + \lambda |\nabla(\bar{U} - U^*)|^2] d\mathbf{x} + \lambda^2 \int_{\partial\Omega} e^{2\lambda r^{-\beta}} |\nabla(\bar{U} - U^*)|^2 d\sigma(\mathbf{x}) + \epsilon \|\bar{U} - U^*\|_H^2 \\ & \leq C \left[\mathbf{M} \int_{\Omega} e^{2\lambda r^{-\beta}} [|\bar{U} - U^*|^2 + |\nabla(\bar{U} - U^*)|^2] d\mathbf{x} \right. \\ & \quad \left. + \lambda^2 \int_{\partial\Omega} e^{2\lambda r^{-\beta}} |\mathbf{h} - \mathbf{h}^*|^2 d\sigma(\mathbf{x}) + \epsilon \|U^*\|_H^2 \right]. \end{aligned} \quad (4.12)$$

Letting λ be sufficiently large, we can use the first integral in the left-hand side of (4.12) to dominate the first integral in the right-hand side of (4.12). We obtain (4.1). \square

Algorithm 1 The procedure to compute numerical solutions to (2.9)

- 1: Choose a regularization parameter ϵ and a threshold number $\kappa_0 > 0$.
 - 2: Set $n = 0$. Choose an arbitrary initial solution $U_0 \in H$.
 - 3: Compute $U_{n+1} = \Phi_{\lambda, \beta, \epsilon}(U_n)$ by minimizing $J_{\lambda, \beta, \epsilon}^{U_n}$ in H .
 - 4: **if** $\|U_{n+1} - U_n\|_{L^2(\Omega)} > \kappa_0$ **then**
 - 5: Replace n by $n + 1$.
 - 6: Go back to Step 3.
 - 7: **else**
 - 8: Set the computed solution $U_{\text{comp}} = U_{n+1}$.
 - 9: **end if**
-

Theorem 4.1 leads to Algorithm 1 to solve the time-reduction model (2.9).

Remark 4.1. *In the statement of Theorem 4.1, we imposed a technical condition regarding the Lipschitz continuity of the nonlinear and nonlocal operator F in (3.4), and consequently, the nonlinear function \mathbf{F} in (3.5). One might thus assume that the Lipschitz condition is a necessary requirement for Algorithm 1 and Algorithm 3. However, this assumption can be relaxed under certain circumstances. Suppose we possess an upper bound on U^* , say $\|U^*\|_{C^1(\bar{\Omega})} \leq M$, where M is a positive constant. In such cases, we only need to compute the solution within the set $\{U \in H : \|U\|_{C^1(\bar{\Omega})} \leq M\}$. To facilitate this, we define the following functions*

$$\chi_M(\mathbf{x}, s, \mathbf{p}) = \begin{cases} 1 & s^2 + |\mathbf{p}|^2 \leq M, \\ \in (0, 1) & M < s^2 + |\mathbf{p}|^2 \leq 2M, \\ 0 & s^2 + |\mathbf{p}|^2 > 2M, \end{cases} \quad \text{and} \quad \mathbf{F}_M = \chi_M \mathbf{F}.$$

It is obvious that U^* satisfies

$$\begin{cases} \Delta U(\mathbf{x}) - SU(\mathbf{x}) + \mathbf{F}_M U(\mathbf{x}) = 0 & \mathbf{x} \in \Omega, \\ U(\mathbf{x}) = 0 & \mathbf{x} \in \partial\Omega, \\ \partial_\nu U(\mathbf{x}) = \mathbf{h}(\mathbf{x}) & \mathbf{x} \in \partial\Omega. \end{cases}$$

We can then compute U^* using Algorithm 1, replacing \mathbf{F} with \mathbf{F}_M . In cases where we do not possess an upper bound for $\|U^*\|_{C^1(\bar{\Omega})}$, we can apply the aforementioned procedure for some value of M to compute U_{comp}^M , and subsequently, let $M \rightarrow \infty$. The convergence of the computed solution is guaranteed as long as the true solution U^* lies within the class C^1 .

5 Numerical study

In this section, we present some numerical examples. The first step to generate the noisy simulated data, see the following subsection.

5.1 Data generation

We consider the case when $d = 2$. Set $\Omega = (-R, R)^d$ where $R = 1$. Fix a number $N_{\mathbf{x}}$. We arrange an $N_{\mathbf{x}} \times N_{\mathbf{x}}$ uniform partition of $\bar{\Omega}$ with the grid points

$$\mathcal{G} = \{\mathbf{x}_{ij} = (-R + (i-1)\delta_{\mathbf{x}}, -R + (j-1)\delta_{\mathbf{x}}) : 1 \leq i, j \leq N_{\mathbf{x}}\} \subset \bar{\Omega}$$

where $\delta_{\mathbf{x}} = \frac{2R}{N_{\mathbf{x}}-1}$. Here, $N_{\mathbf{x}} = 81$. We also discretize the time domain $[0, T]$ by N_T points

$$\mathcal{T} = \{t_l = (l-1)\delta_t : 1 \leq l \leq N_T\}$$

where $\delta_t = \frac{T}{N_T-1}$ for $N_T = 200$ and $T = 2$. To solve the forward problem, we employ a combination of explicit and implicit schemes for $u(x_i, y_j, t_l)$, where $1 \leq i, j \leq N_{\mathbf{x}}$ and $1 \leq l \leq N_T$. The algorithm used to implement this approach is described in Algorithm 2. Solving for w in Step 3 of Algorithm

Algorithm 2 The procedure to generate the data

- 1: Set $u(\mathbf{x}_{ij}, t_1) = u(\mathbf{x}_{ij}, t_2) = g(\mathbf{x}_{ij})$ for $\mathbf{x}_{ij} \in \mathcal{G}$.
- 2: **for** $l = 3$ to N_T **do**
- 3: Solve the boundary value linear elliptic problem

$$\begin{cases} \frac{w-2u(\mathbf{x}, t_{l-1})+u(\mathbf{x}, t_{l-2})}{\delta_t^2} = \Delta w + \mathcal{F}(u(\mathbf{x}, t_{l-1})) & \mathbf{x} \in \mathcal{G}, \\ w(\mathbf{x}) = 0 & \mathbf{x} \in \mathcal{G} \cap \partial\Omega. \end{cases} \quad (5.1)$$

for a function w .

- 4: Set $u(\mathbf{x}, t_l) = w(\mathbf{x})$ for all $\mathbf{x} \in \mathcal{G}$.
- 5: **end for**
- 6: Compute the noisy data

$$h(\mathbf{x}, t_l) = \partial_{\nu} u(\mathbf{x}, t_l)(1 + \delta \text{rand})$$

on $\mathcal{G} \times \mathcal{T}$ where δ is the noise level.

2 is standard since (5.1) is linear with respect to w . One can download a package to solve elliptic PDE with given Dirichlet boundary data on <https://github.com/nhlocnguyenIP/Elliptic> to solve (5.1). In Step 6 of Algorithm 2, the function “rand” gives a uniformly distributed random number in the range $[-1, 1]$. In all of our numerical tests, the noise level δ is 10%.

5.2 The implementation for the inverse problem

Algorithm 3 The procedure solve Problem 1.1

- 1: Choose a cut-off number N .
- 2: Use Algorithm 1 to compute a solution U_{comp} to (2.9).
- 3: Write $U_{\text{comp}} = (u_1^{\text{comp}}, \dots, u_N^{\text{comp}})$. Compute the source function g by the following formula

$$g_{\text{comp}}(\mathbf{x}) = \sum_{n=1}^N u_n^{\text{comp}}(\mathbf{x}) \Psi_n(0)$$

for all $\mathbf{x} \in \Omega$.

The method for calculating the source function g is detailed in Algorithm 3. It is important to note that the initial condition $u_t(\mathbf{x}, 0) = 0$, $\mathbf{x} \in \Omega$, is not explicitly used in the derivation of Algorithm 3. Nevertheless, the uniqueness of Problem 1.1 cannot be assured without the knowledge of $u(\mathbf{x}, 0)$, $\mathbf{x} \in \Omega$. This implies that the solution obtained might not be the desired one, indicating that this condition is implicitly incorporated in our approach.

We interpret our choice of N in Step 1. This choice depends on how good the approximation of the function u and its approximation in (2.1). We, however, the internal information of u is unavailable. We only test the approximation on $\partial\Omega$. Take the data h at a point $\mathbf{x}^* \in \partial\Omega$. For each N , define

$$e_N(t) = \left| h(\mathbf{x}^*, t) - \sum_{n=1}^N h_n(\mathbf{x}^*) \Psi_N(t) \right|$$

where $h_n(x^*) = \int_0^T h(\mathbf{x}^*, t) \Psi_n(t) dt$. A number N is chosen if $\|e_N\|_{L^\infty([0, T])} < \varepsilon$ for some $\varepsilon \ll 1$. In our computation, we choose $\varepsilon = 5 \times 10^{-3}$ and $N = 40$. Figure 1 illustrates this procedure when the data h is taken from Test 1 below.

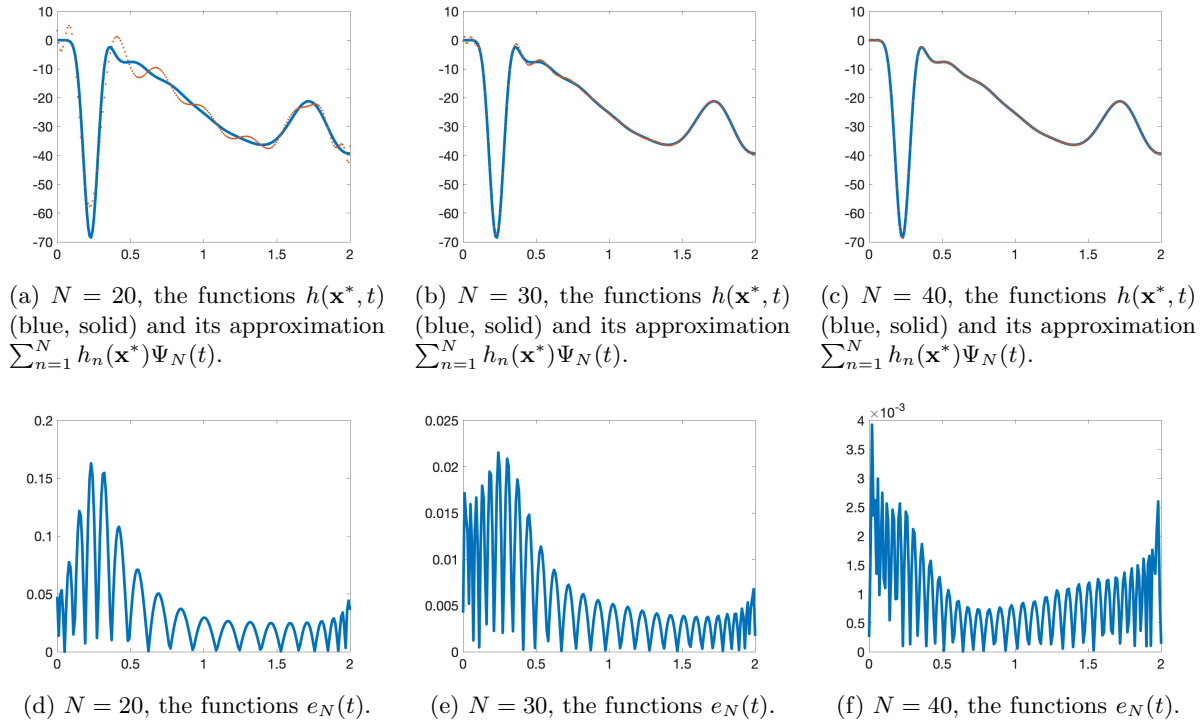


Figure 1: It is evident that when $N = 40$, the data $h(\mathbf{x}^*, \cdot)$ is well approximated by cutting its Fourier series. The function h in these figures is the data for Test 1 in this section. The point $\mathbf{x}^* = (-1, 0)$.

We refer the reader to [47] for the implementation of Step 2. In this step, the parameters $\epsilon = 10^{-13}$, $\lambda = 6$ and $\beta = 10$ are chosen by a trial and error process. We take a reference test (test 1), which we assume to know the true solution. We then run Algorithm 3 with many values of these parameters until we obtain acceptable solutions. We then use these parameters for all other tests. Step 3 is straightforward.

5.3 Numerical examples

We provide three (3) tests.

Test 1. We consider the case when

$$\mathcal{F}(u) = \min \left\{ u^2 + |\nabla u|, 30 \right\} + \int_0^t u(\mathbf{x}, s) ds$$

and the true source function is given by

$$g_{\text{true}}(\mathbf{x}) = \begin{cases} 10 & \text{if } x^2 + 3y^2 < 0.8^2, \\ 0 & \text{otherwise.} \end{cases}$$

The solutions of this test are displayed in Figure 2.

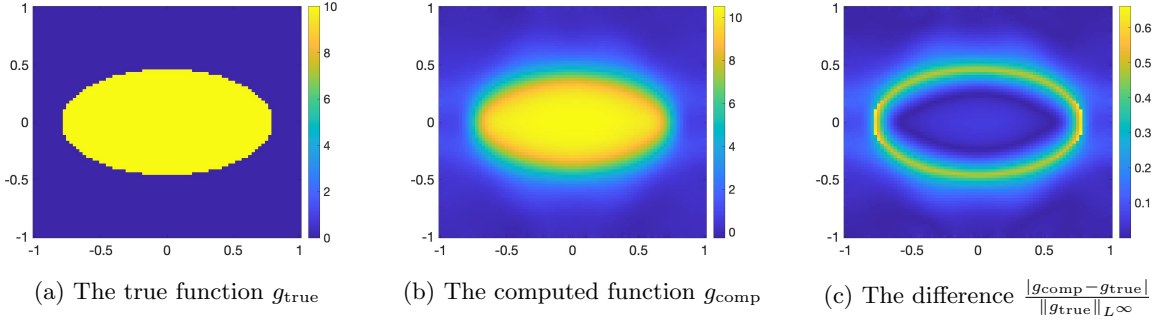


Figure 2: True and numerical solutions of test 1. It is interesting mentioning that although the true solution has a high value (10) and the size of the “ellipse inclusion” is not small, our method can deliver a satisfactory solution without requesting a good initial guess. The error in computation occurs mostly at the boundary of the inclusion.

This test is challenging since the nonlinearity is not smooth. The growth of u is of the quadratic function. It is also interesting with the presence of the nonlocal term. However, it is evident that our method provides a good numerical solution, although this test is complicated. The maximum value of the reconstructed source function g_{comp} in the ellipse inclusion is 10.5148 (the relative error is 5.15%).

Test 2. We test the case when

$$\mathcal{F}(u) = \frac{1}{\sqrt{u^2 + |\nabla u|^2}} + \int_0^t \frac{u(\mathbf{x}, s)}{1 + s^2} ds$$

and the true source function is given by

$$g_{\text{true}}(\mathbf{x}) = \begin{cases} 5 & \text{if } \max\{|x - 0.5|/0.35, |y|/0.8\} < 1, \\ 4 & \text{if } (x + 0.5)^2 + y^2 > 0.35^2, \\ 0 & \text{otherwise.} \end{cases}$$

The support of the true source function consists of two “inclusions”, one rectangle and one disk. The solutions of this test are displayed in Figure 3.

It is evident that our method provides a good numerical solution, although the true source function has two inclusions, in each of which, the source function takes different values. These values are high (5 and 4). The maximum value of the reconstructed source function g_{comp} in the

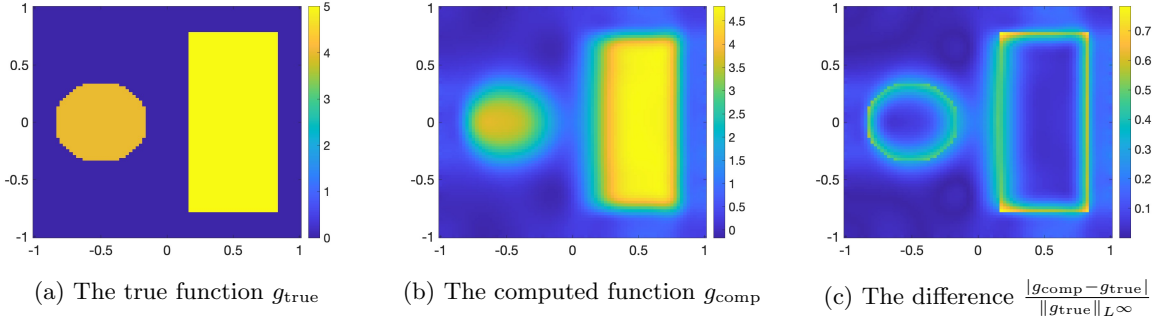


Figure 3: True and numerical solutions of test 2. Like in test 1, our method can deliver a satisfactory solution for test 2 without requesting a good initial guess. Also, the error in computation occurs mostly at the boundary of the inclusion.

rectangular inclusion is 4.8 (the relative error is 3.74%). The maximum value of the reconstructed source function g_{comp} in the circular inclusion is 3.75 (the relative error is 6.25%).

Test 3. We test the case when

$$\mathcal{F}(u) = u \ln(u^2 + 1) + u_x + u_y + \int_0^t u(\mathbf{x}, s) ds$$

and the true source function is given by

$$g_{\text{true}}(\mathbf{x}) = \begin{cases} 7 & \text{if } \max\{|x + 0.6|/0.25, |y - 0.2|/0.7\} < 1, \\ 7 & \text{if } \max\{|x + 0.5|/0.25, |y|/0.7\} < 1, \\ 0 & \text{otherwise.} \end{cases}$$

The support of the true source function is an L shape conclusion. The solutions of this test are displayed in Figure 4.

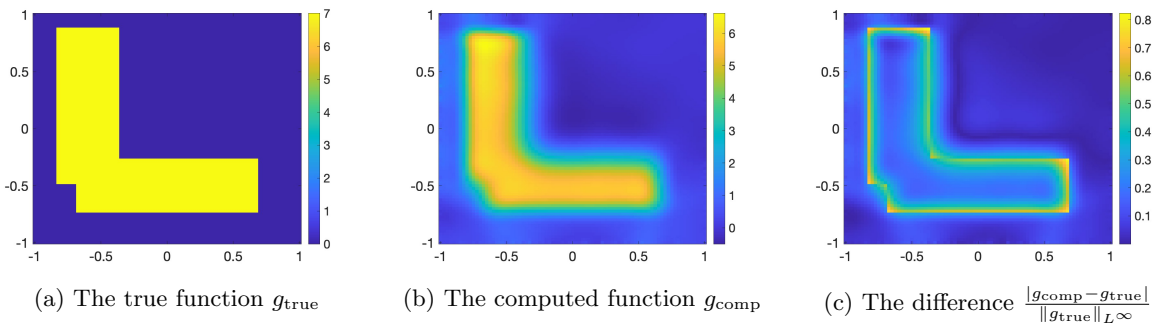


Figure 4: True and numerical solutions of test 3. Like in tests 1 and 2, our method can deliver a satisfactory solution for test 2 without requesting a good initial guess. Also, the error in computation occurs mostly at the boundary of the inclusion.

Although the structure of the true source function is complicated and the value of the function

is high (7), the numerical solution is out of expectation. The maximum value of the reconstructed source function g_{comp} in the L shape inclusion is 6.61 (the relative error is 5.5%).

6 Concluding remarks

The primary objective of this research paper is to tackle the task of computing initial conditions for quasi-linear and nonlocal hyperbolic equations. To achieve this goal, we propose the time dimensional reduction approach that involves approximating the solution of the hyperbolic equation through the truncation of its Fourier expansion in the time domain. By employing the polynomial-exponential basis, we effectively eliminate the time variable, resulting in a transformed system comprising quasi-linear elliptic equations. In order to globally solve this system without the requirement of a well-informed initial guess, we employ the powerful Carleman contraction principle. This principle allows us to navigate the intricacies of the system and derive solutions that meet our objectives. To substantiate the effectiveness of our proposed method, we provide a comprehensive range of numerical examples that showcase its efficacy in practice.

The noteworthy advantage of the time dimensional reduction method extends beyond its ability to deliver accurate solutions. It also boasts exceptional computational speed, which is a significant advantage in addressing complex problems efficiently. We used an iMac with a processor of 3.2 GHz, Intel Core i5 built in 2015 to compute numerical solutions for the tests above. It took about 3.92 minutes including exporting the pictures to complete all tasks of Algorithm 3. The speed is impressive since we can solve a nonlinear and nonlocal problem in $2 + 1$ dimension within a short time.

Acknowledgement

The works of LHN were partially supported by National Science Foundation grants DMS-2208159 and by funds provided by the Faculty Research Grant program at UNC Charlotte Fund No. 111272. The authors extend their gratitude to VIASM and the organizers of the PDE and Related Topics workshop held at VIASM in Hanoi, Vietnam, in July 2022. The initiation of this project took place at this meeting.

References

- [1] A. Abhishek, T. T. Le, L. H. Nguyen, and T. Khan. The Carleman-Newton method to globally reconstruct a source term for nonlinear parabolic equation. *preprint, arXiv:2209.08011*, 2022.
- [2] S. Acosta and B. Palacios. Thermoacoustic tomography for an integro-differential wave equation modeling attenuation. *J. Differential Equations*, 5:1984–2010, 2018.
- [3] H. Ammari, E. Bretin, J. Garnier, and V. Wahab. Time reversal in attenuating acoustic media. *Contemp. Math.*, 548:151–163, 2011.
- [4] H. Ammari, E. Bretin, E. Jugnon, and V. Wahab. Photoacoustic imaging for attenuating acoustic media. In H. Ammari, editor, *Mathematical Modeling in Biomedical Imaging II*, pages 57–84. Springer, 2012.

- [5] A. B. Bakushinskii, M. V. Klibanov, and N. A. Koshev. Carleman weight functions for a globally convergent numerical method for ill-posed Cauchy problems for some quasilinear PDEs. *Nonlinear Anal. Real World Appl.*, 34:201–224, 2017.
- [6] H. Brézis. *Functional Analysis, Sobolev Spaces and Partial Differential Equations*. Springer, New York, 2011.
- [7] P. Burgholzer, H. Grün, M. Haltmeier, R. Nuster, and G. Paltauf. Compensation of acoustic attenuation for high-resolution photoacoustic imaging with line detectors. *Proc. SPIE*, 6437:643724, 2007.
- [8] C. Clason and M. V. Klibanov. The quasi-reversibility method for thermoacoustic tomography in a heterogeneous medium. *SIAM J. Sci. Comput.*, 30:1–23, 2007.
- [9] N. Do and L. Kunyansky. Theoretically exact photoacoustic reconstruction from spatially and temporally reduced data. *Inverse Problems*, 34(9):094004, 2018.
- [10] L. C. Evans. *Partial Differential Equations*. Graduate Studies in Mathematics, Volume 19. Amer. Math. Soc., 2010.
- [11] M. Haltmeier. Inversion of circular means and the wave equation on convex planar domains. *Comput. Math. Appl.*, 65:1025–1036, 2013.
- [12] M. Haltmeier and L. V. Nguyen. Reconstruction algorithms for photoacoustic tomography in heterogeneous damping media. *Journal of Mathematical Imaging and Vision*, 61:1007–1021, 2019.
- [13] M. Hanke, A. Neubauer, and O. Scherzer. A convergence analysis of the Landweber iteration for nonlinear ill-posed problems. *Numer. Math.*, 72:21–37, 1995.
- [14] A. Homan. Multi-wave imaging in attenuating media. *Inverse Probl. Imaging*, 7:1235–1250, 2013.
- [15] Y. Hristova. Time reversal in thermoacoustic tomography—an error estimate. *Inverse Problems*, 25:055008, 2009.
- [16] Y. Hristova, P. Kuchment, and L. V. Nguyen. Reconstruction and time reversal in thermoacoustic tomography in acoustically homogeneous and inhomogeneous media. *Inverse Problems*, 24:055006, 2008.
- [17] C. Huang, K. Wang, L. Nie, L. V. Wang, and M. A. Anastasio. Full-wave iterative image reconstruction in photoacoustic tomography with acoustically inhomogeneous media. *IEEE Trans. Med. Imaging*, 32:1097–1110, 2013.
- [18] V. Katsnelson and L. V. Nguyen. On the convergence of time reversal method for thermoacoustic tomography in elastic media. *Applied Mathematics Letters*, 77:79–86, 2018.
- [19] V. A. Khoa, G. W. Bidney, M. V. Klibanov, L. H. Nguyen, L. Nguyen, A. Sullivan, and V. N. Astratov. Convexification and experimental data for a 3D inverse scattering problem with the moving point source. *Inverse Problems*, 36:085007, 2020.

- [20] V. A. Khoa, G. W. Bidney, M. V. Klibanov, L. H. Nguyen, L. Nguyen, A. Sullivan, and V. N. Astratov. An inverse problem of a simultaneous reconstruction of the dielectric constant and conductivity from experimental backscattering data. *Inverse Problems in Science and Engineering*, 29(5):712–735, 2021.
- [21] V. A. Khoa, M. V. Klibanov, and L. H. Nguyen. Convexification for a 3D inverse scattering problem with the moving point source. *SIAM J. Imaging Sci.*, 13(2):871–904, 2020.
- [22] M. V. Klibanov. Global convexity in a three-dimensional inverse acoustic problem. *SIAM J. Math. Anal.*, 28:1371–1388, 1997.
- [23] M. V. Klibanov. Global convexity in diffusion tomography. *Nonlinear World*, 4:247–265, 1997.
- [24] M. V. Klibanov. Carleman weight functions for solving ill-posed Cauchy problems for quasi-linear PDEs. *Inverse Problems*, 31:125007, 2015.
- [25] M. V. Klibanov. Convexification of restricted Dirichlet to Neumann map. *J. Inverse and Ill-Posed Problems*, 25(5):669–685, 2017.
- [26] M. V. Klibanov and O. V. Ioussoupova. Uniform strict convexity of a cost functional for three-dimensional inverse scattering problem. *SIAM J. Math. Anal.*, 26:147–179, 1995.
- [27] M. V. Klibanov and A. E. Kolesov. Convexification of a 3-D coefficient inverse scattering problem. *Computers and Mathematics with Applications*, 77:1681–1702, 2019.
- [28] M. V. Klibanov, T. T. Le, L. H. Nguyen, A. Sullivan, and L. Nguyen. Convexification-based globally convergent numerical method for a 1D coefficient inverse problem with experimental data. *Inverse Problems and Imaging*, 16:1579–1618, 2022.
- [29] M. V. Klibanov, J. Li, and W. Zhang. Convexification of electrical impedance tomography with restricted Dirichlet-to-Neumann map data. *Inverse Problems*, 35:035005, 2019.
- [30] M. V. Klibanov, J. Li, and W. Zhang. Convexification for an inverse parabolic problem. *Inverse Problems*, 36:085008, 2020.
- [31] M. V. Klibanov, Z. Li, and W. Zhang. Convexification for the inversion of a time dependent wave front in a heterogeneous medium. *SIAM J. Appl. Math.*, 79:1722–1747, 2019.
- [32] M. V. Klibanov, L. H. Nguyen, and H. V. Tran. Numerical viscosity solutions to Hamilton-Jacobi equations via a Carleman estimate and the convexification method. *Journal of Computational Physics*, 451:110828, 2022.
- [33] R. Kowar. On time reversal in photoacoustic tomography for tissue similar to water. *SIAM J. Imaging Sci.*, 7:509–527, 2014.
- [34] R. Kowar and O. Scherzer. Photoacoustic imaging taking into account attenuation. In H. Ammari, editor, *Mathematics and Algorithms in Tomography II, Lecture Notes in Mathematics*, pages 85–130. Springer, 2012.
- [35] R. A. Kruger, P. Liu, Y. R. Fang, and C. R. Appledorn. Photoacoustic ultrasound (PAUS)–reconstruction tomography. *Med. Phys.*, 22:1605, 1995.

- [36] R. A. Kruger, D. R. Reinecke, and G. A. Kruger. Thermoacoustic computed tomography: technical considerations. *Med. Phys.*, 26:1832, 1999.
- [37] O. A. Ladyzhenskaya. *The Boundary Value Problems of Mathematical Physics*. Springer-Verlag, New York, 1985.
- [38] P. N. H. Le, T. T. Le, and L. H. Nguyen. The Carleman convexification method for Hamilton-Jacobi equations on the whole space. *preprint, arXiv:2206.09824*, 2022.
- [39] T. T. Le. Global reconstruction of initial conditions of nonlinear parabolic equations via the Carleman-contraction method. In D-L. Nguyen, L. H. Nguyen, and T-P. Nguyen, editors, *Advances in Inverse problems for Partial Differential Equations*, volume 784 of *Contemporary Mathematics*, pages 23–42. American Mathematical Society, 2023.
- [40] T. T. Le and L. H. Nguyen. A convergent numerical method to recover the initial condition of nonlinear parabolic equations from lateral Cauchy data. *Journal of Inverse and Ill-posed Problems*, 30(2):265–286, 2022.
- [41] T. T. Le and L. H. Nguyen. The gradient descent method for the convexification to solve boundary value problems of quasi-linear PDEs and a coefficient inverse problem. *Journal of Scientific Computing*, 91(3):74, 2022.
- [42] T. T. Le, L. H. Nguyen, T-P. Nguyen, and W. Powell. The quasi-reversibility method to numerically solve an inverse source problem for hyperbolic equations. *Journal of Scientific Computing*, 87:90, 2021.
- [43] T. T. Le, L. H. Nguyen, and H. V. Tran. A Carleman-based numerical method for quasilinear elliptic equations with over-determined boundary data and applications. *Computers and Mathematics with Applications*, 125:13–24, 2022.
- [44] J. L. Lions and E. Magenes. *Non-homogeneous Boundary Value Problems and Applications*. Springer, Berlin, Heidelberg, 1972.
- [45] A. I. Nachman, J. F. Smith III, and R.C. Waag. An equation for acoustic propagation in inhomogeneous media with relaxation losses. *J. Acoust. Soc. Am.*, 88:1584–1595, 1990.
- [46] F. Natterer. Photo-acoustic inversion in convex domains. *Inverse Probl. Imaging*, 6:315–320, 2012.
- [47] L. H. Nguyen. The Carleman contraction mapping method for quasilinear elliptic equations with over-determined boundary data. *Acta Mathematica Vietnamica*, 48:401–422, 2023.
- [48] L. H. Nguyen and M. V. Klibanov. Carleman estimates and the contraction principle for an inverse source problem for nonlinear hyperbolic equations. *Inverse Problems*, 38:035009, 2022.
- [49] L. V. Nguyen. A family of inversion formulas in thermoacoustic tomography. *Inverse Probl. Imaging*, 3:649–675, 2009.
- [50] P. M. Nguyen, T. T. Le, L. H. Nguyen, and M. V. Klibanov. Numerical differentiation by the polynomial-exponential basis. *to appear in Journal of Applied and Industrial Mathematics, preprint arXiv:2304.05909*, 2023.

- [51] A. Oraevsky, S. Jacques, R. Esenaliev, and F. Tittel. Laser-based optoacoustic imaging in biological tissues. *Proc. SPIE*, 2134A:122, 1994.
- [52] G. Paltauf, R. Nuster, M. Haltmeier, and P. Burgholzer. Experimental evaluation of reconstruction algorithms for limited view photoacoustic tomography with line detectors. *Inverse Problems*, 23:S81–S94, 2007.
- [53] G. Paltauf, J. A. Viator, S. A. Prahl, and S. L. Jacques. Iterative reconstruction algorithm for optoacoustic imaging. *J. Opt. Soc. Am.*, 112:1536–1544, 2002.
- [54] P. Stefanov and G. Uhlmann. Thermoacoustic tomography with variable sound speed. *Inverse Problems*, 25:075011, 2009.
- [55] P. Stefanov and G. Uhlmann. Thermoacoustic tomography arising in brain imaging. *Inverse Problems*, 27:045004, 2011.